

Nonlinear transport theory at the order of quantum metric

Zhen-Hao Gong^{†, 1}, Z. Z. Du^{†, 2, 3}, Hai-Peng Sun,⁴ Hai-Zhou Lu,^{1, 5, *} and X. C. Xie^{6, 7, 8}

¹Department of Physics and Guangdong Basic Research Center of Excellence for Quantum Science, Southern University of Science and Technology (SUSTech), Shenzhen 518055, China

²International Quantum Academy, Shenzhen 518048, China

³Shenzhen Key Laboratory of Quantum Science and Engineering, Shenzhen 518055, China

⁴Institute for Theoretical Physics and Astrophysics,

University of Würzburg, 97074 Würzburg, Germany

⁵Quantum Science Center of Guangdong-Hong Kong-Macao Greater Bay Area (Guangdong), Shenzhen 518045, China

⁶Interdisciplinary Center for Theoretical Physics and Information Sciences (ICTPIS), Fudan University, Shanghai 200433, China

⁷International Center for Quantum Materials, School of Physics, Peking University, Beijing 100871, China

⁸Hefei National Laboratory, Hefei 230088, China

(Dated: October 8, 2024)

Quantum metric, a probe to spacetime of the Hilbert space, has been found measurable in the nonlinear electronic transport and attracted tremendous interest. We show that the quantum metric is only a tip of the iceberg, by deriving unknown 11 out of 14 formulas of the quadratic nonlinear conductivity under the same symmetry that the quantum metric emerges. The formulas allow us to determine nonzero nonlinear conductivity elements for the magnetic point groups, calculate the quadratic nonlinear conductivity for arbitrary Hamiltonian, e.g., the even-layered MnBi_2Ti_4 thin films with and without the C_3 symmetry, and formulate scaling laws at the order of quantum metric to distinguish different mechanisms in the recent experiments. The theory is a comprehensive description of the quadratic nonlinear transport and will facilitate future experiments and applications.

Introduction.— The nonlinear Hall effect is characterized by a transverse voltage nonlinearly dependent on the longitudinal driving current. It has received tremendous attention because of its potential as a measurement method and for device applications [1–29]. More excitingly, without time-reversal and inversion symmetries but under a combined time-reversal and inversion symmetry, the nonlinear Hall effect can be contributed by the quantum metric [30–35], the real part of quantum geometry [36–40], which measures the distance between quantum states, thus can provide spacetime insight to the challenges in condensed matter [41]. The nonlinear Hall effect from the quantum metric dipole (χ^{QMD} and \mathcal{G}_l^{ab} in Tab. I) is essentially an anomalous Hall effect but with the driving current acting twice. In this sense, the disorder contributions, such as the side-jump and skew-scattering [42], cannot be ignored [6], inspiring an increasing interest in exhausting all contributions to the nonlinear transport [43, 44].

In this Letter, we try to formulate all the contributions to the quadratic nonlinear conductivities under the same symmetry that the quantum metric emerges, by treating the geometry and disorder on the same footing. We find 11 out of 14 conductivity formulas unknown in the literature. The formulas allow a symmetry analysis to determine nonzero nonlinear conductivity elements for the magnetic point groups at the order of quantum metric. By applying the formulas to even-layered MnBi_2Te_4 thin films as those in the experiments [33, 34], we find that the disorder-induced contributions could be comparable with the quantum metric part, even stronger by orders of mag-

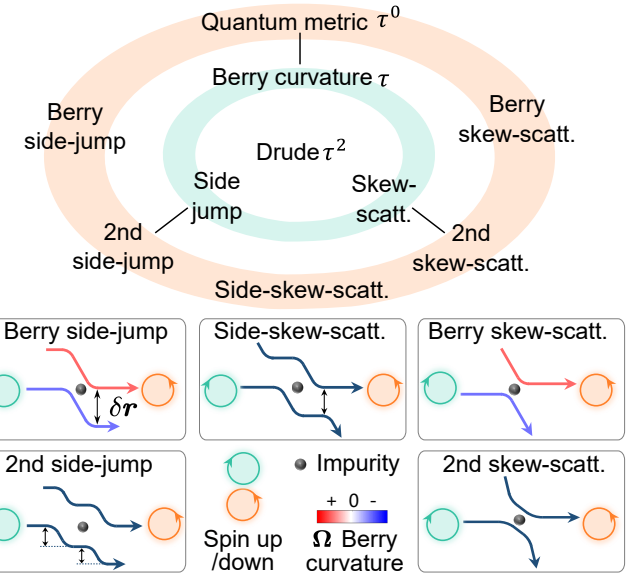


FIG. 1. Hierarchy of the quadratic nonlinear transport, including (i) the Drude mechanism in absence of time reversal and inversion symmetries, (ii) the Berry curvature dipole [1, 2], side-jump, and skew-scattering mechanisms [6, 11] under time-reversal but without inversion symmetry, and (iii) the quantum metric dipole (Berry connection polarizability) [30–32] and mixed Berry and skew-scattering contributions [43], as well as 2nd-order side-jump, 2nd-order skew-scattering, mixed Berry-side-jump, and mixed side-jump-skew-scattering revealed in this work, in absence of time-reversal and inversion symmetries but under a combined time-reversal and inversion symmetry. They can also be roughly categorised by the power law of the scattering time τ . The color bar indicates the Berry curvature Ω .

TABLE I. Formulas of the quadratic nonlinear conductivity at the order of quantum metric, including the quantum metric dipole (QMD), Drude, mixed Berry curvature and skew-scattering (BSK), mixed Berry curvature and side-jump (BSJ), second-order side-jump (2SJ) and skew-scattering (2SK), mixed side-jump and skew-scattering (SSK). τ is the scattering time, $-e$ is the electron charge, ε^{abc} is the anti-symmetric tensor, Fermi distribution $f_l^{(0)} = 1/[\exp[(\epsilon_l - \epsilon_F)/k_B T] + 1]$ with the Fermi energy ϵ_F , l stands for the band index γ and wave vector $\mathbf{k} = |k|e^{i\phi}$, Ω_l^a is the Berry curvature [45], \mathcal{G}_l^{ab} is the Berry connection polarizability tensor, which is related to the quantum metric tensor $\text{Re}(A_a^{\gamma\gamma'} A_b^{\gamma'\gamma})$ for two-band cases [30–32], Berry connection $A_a^{\gamma\gamma'} \equiv i(\gamma|\partial_{\mathbf{k}}^a|\gamma')$ [45], $\partial_{\mathbf{k}}^b \equiv \partial/\partial k_b$, $\hat{\mathcal{H}}$ is the Hamiltonian, ϵ_l is the eigen energy, group velocity $v_l^a = (1/\hbar)\partial\epsilon_l/\partial k_a$, $\partial_{\epsilon_l} \equiv \partial/\partial\epsilon_l$, side-jump velocity $v_l^{sj,a} = \sum_l \varpi_{ll'}^S \delta r_{ll'}^a$, $\varpi_{ll'}^S$ ($\varpi_{ll'}^A$) is the symmetric (anti-symmetric) scattering rate between states l and l' (Sec. SIB of [46]), $\delta r_{ll'}^a$ is the coordinates shift with $V_{ll'} = \langle l|\hat{V}_{imp}|l'\rangle$ [6, 47], where the δ -correlated random potential $\hat{V}_{imp}(\mathbf{r}) = \sum_i V_i \delta(\mathbf{r} - \mathbf{R}_i)$ can give the Gaussian $\langle V_i^2 \rangle_{dis} = V_0^2$ and non-Gaussian correlations $\langle V_i^3 \rangle_{dis} = V_1^3$ [6, 11, 47], leading to the Gaussian (intrinsic skew-scattering) $\varpi_{ll'}^{(4A)}$ and non-Gaussian (extrinsic skew-scattering) $\varpi_{ll'}^{(3A)}$ parts to $\varpi_{ll'}^A$. $\bar{O}_{ll'}^a$ ($\hat{O}_{ll'}^a$) is the symmetric (anti-symmetric) part of $O_{ll'}^a$ [6], and $T_{ll'}$ is the T-matrix [48] (details in Secs. SI and SII of [46]).

Known (3 out of 14)

$$\begin{aligned} \chi^{\text{QMD}} &= e^2 \sum_l (v_l^a \mathcal{G}_l^{bc} - v_l^b \mathcal{G}_l^{ac}) \partial_{\epsilon_l} f_l^{(0)} \quad [30-32], \\ \chi^{\text{Drude}} &= -\frac{\tau^2 e^3}{2\hbar^2} \sum_l v_l^a \partial_{\mathbf{k}}^b \partial_{\mathbf{k}}^c f_l^{(0)} \quad [1], \\ \chi_1^{\text{BSK}} &= \frac{\tau^2 e^3}{2\hbar^2} \sum_{ll'} \varepsilon^{acd} \Omega_{l'}^d \varpi_{ll'}^{(3A)} \partial_{\mathbf{k}}^b f_l^{(0)} \quad [43], \end{aligned}$$

where

$$\begin{aligned} \mathcal{G}_l^{ab} &\equiv 2e \text{Re} \sum_{\gamma' \neq \gamma} A_a^{\gamma\gamma'} A_b^{\gamma'\gamma} / (\varepsilon_{\mathbf{k}}^{\gamma} - \varepsilon_{\mathbf{k}}^{\gamma'}), \\ \Omega_l^a &\equiv -2\varepsilon^{abc} \sum_{\gamma' \neq \gamma} \text{Im} \langle \gamma | \partial_{\mathbf{k}}^b \hat{\mathcal{H}} | \gamma' \rangle \langle \gamma' | \partial_{\mathbf{k}}^c \hat{\mathcal{H}} | \gamma \rangle / (\varepsilon_{\mathbf{k}}^{\gamma} - \varepsilon_{\mathbf{k}}^{\gamma'})^2, \\ \delta r_{ll'}^a &\equiv i \langle l | \partial_{\mathbf{k}}^a | l' \rangle - i \langle l' | \partial_{\mathbf{k}}^a | l \rangle - (\partial_{\mathbf{k}}^a + \partial_{\mathbf{k}}^a) \arg(V_{ll'}), \\ O_{ll'}^a &\equiv (2\pi/\hbar) |T_{ll'}| \delta r_{ll'}^a \partial_{\epsilon_l} \delta(\epsilon_l - \epsilon_{l'}), \\ 1/\tau &\approx 1/\tau_{\mathbf{k}} \equiv \sum_{\mathbf{k}'} \varpi_{\mathbf{k}\mathbf{k}'}^{(2)} [1 - \cos(\phi - \phi')] \delta(\epsilon_F - \epsilon_l). \end{aligned}$$

This work (11 out of 14)

$$\begin{aligned} \chi_2^{\text{BSK}} &= \frac{\tau^2 e^3}{2\hbar^2} \sum_{ll'} \varepsilon^{acd} \Omega_{l'}^d \varpi_{ll'}^{(4A)} \partial_{\mathbf{k}}^b f_l^{(0)}, \\ \chi^{\text{BSJ}} &= \frac{\tau e^3}{2\hbar} \sum_l \varepsilon^{acd} \Omega_l^d v_l^{sj,b} \partial_{\epsilon_l} f_l^{(0)}, \\ \chi_1^{\text{2SK}} &= \frac{e^3 \tau^4}{2\hbar^2} \sum_{ll'} v_{ll'}^a (\partial_{\mathbf{k}}^c v_{ll'}^a) \varpi_{ll'}^A \varpi_{ll'}^A \partial_{\mathbf{k}}^b f_l^{(0)}, \\ \chi_2^{\text{2SK}} &= \frac{e^3 \tau^4}{2\hbar^2} \sum_{ll'} v_{ll'}^a v_{ll'}^a (\partial_{\mathbf{k}}^c - \partial_{\mathbf{k}}^c) \varpi_{ll'}^A \varpi_{ll'}^A \partial_{\mathbf{k}}^b f_l^{(0)}, \\ \chi_1^{\text{2SJ}} &= \frac{\tau^2 e^3}{2\hbar} \sum_{ll'} (v_l^a + v_l^a) \bar{O}_{ll'}^c v_l^{sj,b} \partial_{\epsilon_l} f_l^{(0)}, \\ \chi_2^{\text{2SJ}} &= \frac{\tau^2 e^3}{2\hbar} \sum_{ll'} (v_l^{sj,a} + v_{l'}^{sj,a}) \bar{O}_{ll'}^c \partial_{\mathbf{k}}^b f_l^{(0)}, \\ \chi_3^{\text{2SJ}} &= -\frac{\tau^2 e^3}{2\hbar} \sum_l \partial_{\mathbf{k}}^b v_l^{sj,a} v_l^{sj,c} \partial_{\epsilon_l} f_l^{(0)}, \\ \chi_1^{\text{SSK}} &= \frac{\tau^2 e^3}{2\hbar} \sum_{ll'} (v_l^a + v_{l'}^a) \bar{O}_{ll'}^c \partial_{\mathbf{k}}^b f_l^{(0)}, \\ \chi_2^{\text{SSK}} &= \frac{\tau^3 e^3}{2\hbar} \sum_{ll'} v_{ll'}^a (v_{ll'}^a + v_{l'}^a) \varpi_{ll'}^A \bar{O}_{ll'}^c \partial_{\mathbf{k}}^b f_l^{(0)}, \\ \chi_3^{\text{SSK}} &= \frac{\tau^3 e^3}{2\hbar} \sum_{ll'} v_{ll'}^a v_{ll'}^a (\varpi_{ll'}^A + \varpi_{ll'}^A) v_{ll'}^a \bar{O}_{ll'}^c \partial_{\mathbf{k}}^b f_l^{(0)} \\ &\quad + \frac{\tau^3 e^3}{2\hbar} \sum_{ll'} v_{ll'}^a v_{ll'}^a v_{ll'}^{sj,b} (\partial_{\mathbf{k}}^c - \partial_{\mathbf{k}}^c) \varpi_{ll'}^A \partial_{\epsilon_l} f_l^{(0)}, \\ \chi_4^{\text{SSK}} &= \frac{\tau^3 e^3}{2\hbar^2} \sum_{ll'} v_{ll'}^{sj,a} (\partial_{\mathbf{k}}^c - \partial_{\mathbf{k}}^c) \varpi_{ll'}^A \partial_{\mathbf{k}}^b f_l^{(0)}. \end{aligned}$$

nitude in the clean limit. The formulas also help to extend the scaling law to the order of quantum metric, that is, the relation between linear longitudinal and nonlinear transverse resistivities, which is crucial for distinguishing mechanisms contributing to the nonlinear transport. This theory is not only at the order of quantum metric but a comprehensive description of the quadratic nonlinear transport under various symmetries.

Quadratic conductivity formulas at the order of quantum metric.— Experimentally, the nonlinear transport is measured as a double-frequency longitudinal or transverse voltage, in response to low frequency (10-1000 Hz) driving currents. Theoretically, it is equivalent to calculate double-frequency current density

$$J_a(2\omega) = \chi_{abc} E_b(\omega) E_c(\omega), \quad (1)$$

in response to low-frequency ($\omega\tau \ll 1$) electric fields E_b, E_c , where $a, b, c \in \{x, y, z\}$. To treat the geometry and disorder contributions on the same footing, we adopt the semiclassical theory [6, 47] to calculate the nonlinear conductivity χ_{abc} (Secs. SI and SII of [46]), in which each contribution has a clear physical origin, as shown by the hierarchy in Fig. 1. The calculation starts with the uniform Boltzmann equation $\partial f_l/\partial t + \dot{\mathbf{k}} \cdot \partial f_l/\partial \mathbf{k} = \mathcal{I}_{el}\{f_l\}$ of the distribution function f_l , where $\mathcal{I}_{el}\{f_l\}$ accounts for the elastic disorder scattering, l stands for the band index γ and wave vector \mathbf{k} , $\dot{\mathbf{k}} = -(e/\hbar)\mathbf{E}$, and \mathbf{E} is the electric

field. By decoupling the distribution function and scattering according to different mechanisms (*in* for disorder-irrelavent, *sj* and *sk* for side-jump and skew-scattering, respectively)

$$\begin{aligned} f_l &= f_l^{in} + \delta f_l^{sj} + \delta f_l^{sk} + \delta f_l^{2sj} + \delta f_l^{2sk} + \delta f_l^{sk,sj}, \\ \mathcal{I}_{el}\{f_l\} &= \mathcal{I}^{in} + \mathcal{I}^{sj} + \mathcal{I}^{sk} + \mathcal{I}^{sk,sj}, \end{aligned} \quad (2)$$

the distribution function can be found up to the second order of the electric field, where $\delta f_l^{2sj} + \delta f_l^{2sk} + \delta f_l^{sk,sj}$ and $\mathcal{I}^{sk,sj}$ are crucial for new findings. Finally, the nonlinear conductivity χ_{abc} can be extracted from the electric current $\mathbf{J}(\mathbf{E}) = -e \sum_l \dot{\mathbf{r}}_l f_l$, where the velocity $\dot{\mathbf{r}}_l = \mathbf{v}_l - \dot{\mathbf{k}} \times \Omega_l + \dot{\mathbf{k}} \times \nabla_{\mathbf{k}} \times \mathbf{G}\mathbf{E} + \mathbf{v}_l^{sj}$ includes the components from the group velocity \mathbf{v}_l , Berry curvature $\mathbf{\Omega}$ [45], Berry connection polarizability \mathbf{G} (related to the quantum metric) [30–32], and side-jump velocity \mathbf{v}^{sj} .

At the order of quantum metric, we find that the quadratic conductivity χ_{abc} can be decomposed into

$$\begin{aligned} \chi_{abc} &= \sum_{i=1}^2 \chi_i^{\text{2SK}} + \sum_{i=1}^3 \chi_i^{\text{2SJ}} + \sum_{i=1}^4 \chi_i^{\text{SSK}} + \chi^{\text{BSJ}} + \chi_2^{\text{BSK}} \\ &\quad + \chi_1^{\text{BSK}} + \chi^{\text{Drude}} + \chi^{\text{QMD}}, \end{aligned} \quad (3)$$

where the first row is our finding, including 11 formulas at the order of quantum metric, as compared in Tab. I with 3 known contributions on the second row. The first

row can survive the same symmetry that the quantum metric dipole χ^{QMD} emerges in the nonlinear transport (see Sec. SIIIA of [46]), i.e., no time-reversal and inversion symmetries but under a combined time-reversal and inversion symmetry. Alternatively, the calculation can be based on the density matrix [44, 49–51], but does not give formulas as those in Tab. I. Below, we show that the explicit form of the formulas is crucial.

TABLE II. Nonzero quadratic conductivity elements χ_{abb} on the x - y plane (defined as $J_a = \chi_{abb}E_b^2$, $\{a, b\} \in \{x, y\}$, abb is short for χ_{abb}) at the order of quantum metric (all formulas in Tab. I), can be found for only 9 out of the 122 magnetic point groups. The quantum metric dipole (QMD) [30–32] as well as BSJ and BSK in this work have the anti-symmetric constraint $\chi_{abc} = -\chi_{cba}$ [11], so they have less nonzero elements than 2SJ, 2SK, and SSK found in this work [52]. The C_2 axis is assumed in order as the y - and x -axis, the mirror plane σ_v is assumed in order as the zx - and yz -plane, and the mirror plane σ_h is assumed as the x - y plane. We use the MGCorep codes [53] to filter the groups without time-reversal and inversion but with the combined time-reversal and inversion symmetry and find their matrices.

Groups	This work	QMD
$\bar{1}', 2'/m$	$xxx \quad xyy$ $yxx \quad yyy$	$yxx \quad xyy$
$2/m', m'\text{mm}$	$yxx \quad yyy$	yxx
$\bar{3}'m, \bar{3}'m', 6'/mmm'$	$yxx = -yyy$	\times
$\bar{3}', 6'/m$	$xyy = -xxx$ $yxx = -yyy$	\times

Nonzero quadratic conductivity elements at quantum metric order for magnetic point groups.— With the help of the above formulas, we can determine the non-zero quadratic nonlinear conductivity elements for the magnetic groups to facilitate experimental verification (details in Sec. SIIIB of [46]). At the order of quantum metric, the system has to break inversion and time-reversal symmetries but preserve the combined time-reversal and inversion symmetry, narrowing the candidates to only 21 out of a total of 122 magnetic point groups. Take the nonzero elements on the x - y plane for the $\bar{3}'m'$ groups for example. One of the symmetry operators is $C_3\mathcal{PT}$, which can be expressed as a matrix \mathcal{R} that rotates the Cartesian coordinates and a matrix \mathcal{Q} that acts on the components of the quadratic electric fields $\{E_x^2, 2E_xE_y, E_y^2\}$. Applying the $C_3\mathcal{PT}$ operation to $J_a = \chi_{abb}E_bE_b$ is equivalent to $\chi = \mathcal{R}\chi\mathcal{Q}^{-1}$, from which the relations $\chi_{yxx} = -\chi_{yyy}$ and $\chi_{xyy} = -\chi_{xxx}$ can be found, as well as $\chi_{abb}^{\text{QMD}} = 0$ because the anti-symmetric part $\chi_{aaa}^{\text{QMD}} = 0$ (details in Sec. SIIIB of [46]). The procedure is applied to all symmetry operations in the $\bar{3}'m'$ group, and the common relations give rise to the nonzero quadratic conductivity elements χ_{abb} on the x - y plane ($\{a, b\} \in \{x, y\}$) as well as their relations, as shown in Tab. II for only 9 out of the 122 magnetic point groups. Only 20 magnetic point

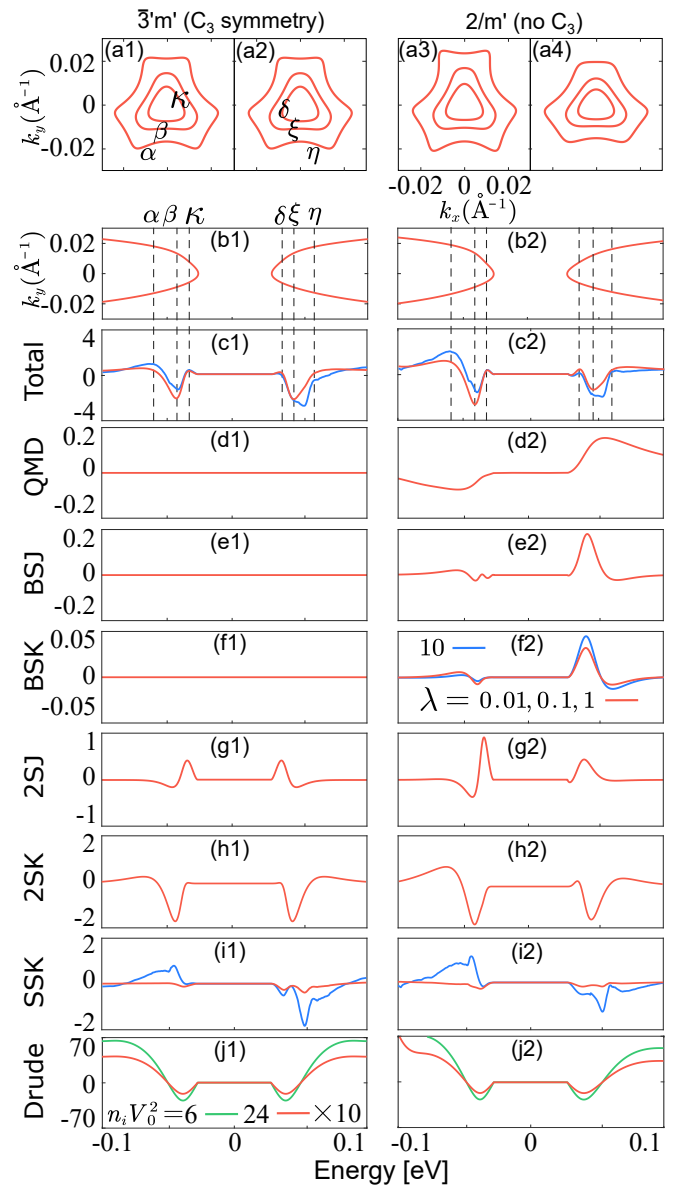


FIG. 2. For the even-layered MnBi_2Te_4 models with and without the C_3 symmetry ($\bar{3}'m'$ and $2/m'$ groups) in Eq. (4), the Fermi surfaces (a1)–(a2), energy bands (b1)–(b2), total quadratic Hall conductivity χ_{yxx} in units of $\text{mA} \cdot \text{nm} \cdot \text{V}^{-2}$ at the order of quantum metric (Drude not included) (c1)–(c2), and the splits of the contributions (d1)–(j2) defined in Eq. (3). Disorder is measured in terms of $\lambda \equiv n_i V_0^3 / (n_i V_0^2)^2$, where n_i is the impurity density, V_0^2 and V_0^3 measures the correlations of two (three) scattering events. The legends in the BSK panel (f2) indicate that the results are almost the same for $\lambda = 0.01, 0.1, 1$, and becomes much stronger as λ goes beyond 10. Parameters are $\gamma = 3.1964 \text{ eV} \cdot \text{\AA}$, $E_0 = 0 \text{ eV}$, $D = 0 \text{ eV}$, $\Delta = -9.21 \text{ meV}$, $B = 1.545 \text{ eV} \cdot \text{\AA}^2$, $m_2 = 27.3 \text{ meV}$, $\beta_1 = 8000 \text{ eV} \cdot \text{\AA}^3$, $s_1 = 0.1 \text{ eV} \cdot \text{\AA}^2$, $s_3 = 50 \text{ eV} \cdot \text{\AA}^2$, $s_5 = 0.1 \text{ eV} \cdot \text{\AA}$, $s_7 = 0.1 \text{ eV} \cdot \text{\AA}$, $s_8 = 0.1 \text{ eV} \cdot \text{\AA}$ [33, 54]. The scattering time τ is evaluated using the vertex-corrected Fermi golden rule (Sec. SIB of [46]). $n_i V_0^2$ in (j1)–(j2) is in units of $\text{eV}^2 \cdot \text{\AA}^2$, $n_i V_0^2 = 6$ gives $\tau \sim 40 \text{ fs}$ as those in the experiment [33], while $n_i V_0^2 = 24$ gives a χ^{Drude} ($\times 10$ in (j1)–(j2)) comparable to other contributions. The Drude part can be filtered using the property $\chi_{yxx}^{\text{Drude}} = \chi_{xyx}^{\text{Drude}}$ [11, 31].

groups have nonzero quadratic conductivity elements in 3D (χ_{abc} , $a, b, c \in \{x, y, z\}$) (see Tabs. S6-S12 of [46]).

MnBi₂Te₄ films with and without C₃ symmetry.— To test our formulas, we consider MnBi₂Te₄ thin films with and without the C₃ symmetry (Sec. SIV of [46]), because the C₃ symmetry forbids conductivity on the x-y plane with anti-symmetric labels, i.e., $\chi_{abc} = -\chi_{cba}$, ($\{a, b, c\} \in \{x, y\}$) [11]. The minimal Hamiltonian reads

$$\hat{\mathcal{H}} = \hat{\mathcal{H}}_0 + \hat{\mathcal{H}}_S, \quad (4)$$

where the C₃ symmetric part [54] $\hat{\mathcal{H}}_0 = h_0 + h_k \hat{\tau}_z \hat{\sigma}_z - \gamma k_x \hat{\tau}_0 \hat{\sigma}_y + \gamma k_y \hat{\tau}_0 \hat{\sigma}_x + m_k \hat{\tau}_x \hat{\sigma}_z$, the Pauli matrices $\hat{\tau}$ and $\hat{\sigma}$ describe orbital and spin degrees of freedom, respectively, $h_0 = E_0 - Dk^2$, k_x and k_y are wave vectors, $k^2 \equiv k_x^2 + k_y^2$, $h_k = \Delta/2 - Bk^2$, $m_k = m_2 + \beta_1 (3k_x^2 k_y - k_y^3)$, E_0 , D , Δ , B , m_2 , β_1 , and γ are model parameters. The C₃-symmetry-breaking part reads [33] $\hat{\mathcal{H}}_S = (s_1 + s_3)k_y^2 \hat{\tau}_0 \hat{\sigma}_0/2 + (s_1 - s_3)k_y^2 \hat{\tau}_z \hat{\sigma}_z/2 - s_5 k_y \hat{\tau}_0 \hat{\sigma}_y + s_7 k_y \hat{\tau}_x \hat{\sigma}_z + s_8 k_x \hat{\tau}_y \hat{\sigma}_z$, where s_1 , s_3 , s_5 , s_7 , and s_8 are model parameters. The model is also classified into the 3'/m' and 2/m' magnetic point groups, respectively, as shown by the Fermi surfaces and energy bands in Fig. 2 (a1)-(b2). Figure 2 (c1)-(j2) shows the total and splits of contributions to the quadratic nonlinear conductivity at the order of quantum metric as functions of the Fermi energy, by applying the formulas in Tab. I to the model in Eq. (4). Several features verify the formulas. (i) The C₃ symmetry cancels χ^{QMD} [31, 32], which can be recovered by the strain that breaks the C₃ symmetry [33]. Our BSJ and BSK also vanish (emerge) under (without) the C₃ symmetry, consistent with the analysis in Tab. II. (ii) The contributions of QMD, BSJ, BSK are comparable, but 2SJ, 2SK, and SSK could overwhelm QMD by orders, when the parameter

$$\lambda \equiv n_i V_1^3 / (n_i V_0^2)^2 \propto 1/n_i \quad (5)$$

is large (n_i is small, i.e., the clean limit), where n_i is the impurity density, V_0^2 (V_1^3) measures the correlations of two (three) scattering events. χ^{QMD} , χ^{BSJ} , χ^{BSK} , and χ^{2SJ} do not depend on λ , χ^{BSK} and χ^{2SJ} are linear in λ , χ^{SSK} has terms $\propto \lambda^0$ and λ^1 , χ^{2SK} has terms $\propto \lambda^0$, λ^1 , and λ^2 (Tab. S5 of [46]). The Drude contribution [1, 31] depends on $1/(n_i V_0^2)^2$. Also, for χ_{xyy} of a specific model, the disorder-induced but disorder-strength-independent contributions could overwhelm the quantum metric part [44].

Scaling law at the order of quantum metric.— The scaling law is powerful in distinguishing mechanisms in the Hall effects [6, 10, 16, 18, 42, 55, 56]. The formulas in Tab. I allow us to extend the scaling law of the nonlinear Hall effect to the order of quantum metric (details in Sec. SV of [46]), characterized by the relation between the nonlinear Hall conductivity χ_{yxx} and longitudinal linear conductivity σ_{xx} as

$$\chi_{yxx} = \mathcal{C}_2 \sigma_{xx}^2 + \mathcal{C}_1 \sigma_{xx} + \mathcal{C}_0, \quad (6)$$

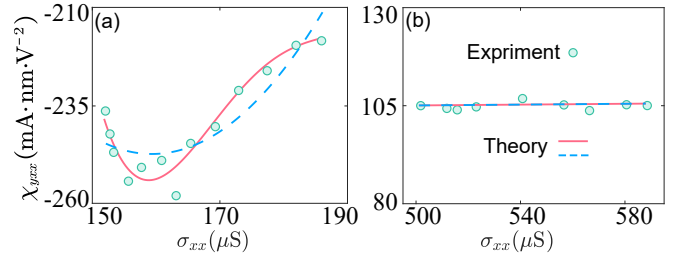


FIG. 3. Scaling laws between the quadratic Hall conductivity χ_{yxx} and linear longitudinal conductivity σ_{xx} for the experimental data (circles) of (a) 4SL [34] and (b) BP-6SL [33] MnBi₂Te₄ thin films (SL for septuple layer, BP for black phosphorous), fitted using Eqs. (6) (solid) and (7) (dashed, details in Fig. S3 of [46]). The fitting parameters in (a) $\mathcal{C}_2 = 5.05 \times 10^4$ mA · nm, $\mathcal{C}_1 = -1.61 \times 10^4$ nm · V⁻¹, $\mathcal{C}_0 = 1.03 \times 10^3$ mA · nm · V⁻¹, and in (b) $\mathcal{C}_2 = 6.98$, $\mathcal{C}_1 = -3.38$, $\mathcal{C}_0 = 1.05 \times 10^2$, with the same units as those in (a). The data in (b) is multiplied by 8 nm to be treated as a 2D case.

where in experiments $\chi_{yxx} = [V_y^{2\omega} \sigma_{xx} / (V_x^\omega)^2] (L^2/W)$, with L the length, W the width in 2D or cross-sectional area in 3D, as well as the transverse double-frequency voltage $V_y^{2\omega}$ and longitudinal single-frequency voltage V_x^ω . The 3 fitting parameters \mathcal{C}_a have physical meanings, as categorized in Tab. III.

TABLE III. Classification of the fitting parameters in the scaling law Eq. (6) by the mechanisms in Fig. 1 and Tab. I and their dependence on the impurity density n_i . The superscripts (3A) and (4A) indicate how many times the anti-symmetric scattering rates $\varpi_{ll'}^{(3A)} \sim n_i V_1^3$ and $\varpi_{ll'}^{(4A)} \sim (n_i V_0^2)^2$ from $\varpi_{ll'}^A$, appear in the formulas of $\chi_{1,2,3,4}^{\text{2SK}}$ and $\chi_{1,2}^{\text{SSK}}$.

Param.	Mechanisms
$\mathcal{C}_2 \sim n_i^{-2}$	$\chi_{1,2}^{\text{2SK}(3A,3A)}, \chi^{\text{Drude}}$
$\mathcal{C}_1 \sim n_i^{-1}$	$\chi_1^{\text{BSK}}, \chi_{1,2}^{\text{2SK}(3A,4A)}, \chi_{1,2,3,4}^{\text{SSK}(3A)}$
$\mathcal{C}_0 \sim n_i^0$	$\chi_2^{\text{BSK}}, \chi_{1,2}^{\text{BSJ}}, \chi_{1,2,3}^{\text{2SJ}}, \chi_{1,2}^{\text{2SK}(4A,4A)}, \chi_{1,2,3,4}^{\text{SSK}(4A)}, \chi_{1,2,3,4}^{\text{QMD}}$

The fitting in Fig. 3 with Eq. (6) shows that all terms are competing from 2 to 10 K in 4SL-layered MnBi₂Te₄ [34], e.g., at $\sigma_{xx} = 170 \mu\text{S}$, $\mathcal{C}_2 \sigma_{xx}^2 = 1.46 \times 10^3$, $\mathcal{C}_1 \sigma_{xx}^1 = -2.73 \times 10^3$, and $\mathcal{C}_0 = 1.03 \times 10^3$; and from 2 to 15 K in BP-6SL-MnBi₂Te₄ thin films [33], the \mathcal{C}_0 term is dominant, e.g., at $\sigma_{xx} = 540 \mu\text{S}$, $\mathcal{C}_2 \sigma_{xx}^2 = 2.04$, $\mathcal{C}_1 \sigma_{xx}^1 = -1.84$, and $\mathcal{C}_0 = 105$. Nevertheless, all mechanisms could contribute in \mathcal{C}_0 . The scaling law Eq. (6) considers only the static scattering. If the dynamic scattering (e.g., due to phonons) is also included, the scaling law becomes

$$\chi_{yxx} = \mathcal{C}'_4 \sigma_{xx}^4 + \mathcal{C}'_3 \sigma_{xx}^3 + \mathcal{C}'_2 \sigma_{xx}^2 + \mathcal{C}'_1 \sigma_{xx} + \mathcal{C}'_0, \quad (7)$$

and the fitting results show more detailed and entangled origins of mechanism (see Fig. S3 of [46]). A similar scaling law is found [57], but no explicit conductivity formulas are given as those in Tab. I and the parameters are not classified according to the physical mechanisms in Fig. 1 and Tab. III.

[†]Z. H. Gong and Z. Z. Du contributed equally. This work was supported by the National Key R&D Program of China (2022YFA1403700), Innovation Program for Quantum Science and Technology (2021ZD0302400), the National Natural Science Foundation of China (11925402, 12374041, 12350402), Guangdong Basic and Applied Basic Research Foundation (2023B0303000011), Guangdong province (2020KCXTD001), the Science, Technology and Innovation Commission of Shenzhen Municipality (ZDSYS20190902092905285), and Center for Computational Science and Engineering of SUSTech.

* Corresponding author: luhz@sustech.edu.cn

[1] I. Sodemann and L. Fu, “Quantum nonlinear Hall effect induced by Berry curvature dipole in time-reversal invariant materials”, *Phys. Rev. Lett.* **115**, 216806 (2015).

[2] T. Low, Y. Jiang, and F. Guinea, “Topological currents in black phosphorus with broken inversion symmetry”, *Phys. Rev. B* **92**, 235447 (2015).

[3] Q. Ma, S.-Y. Xu, H. Shen, D. MacNeill, V. Fatemi, T.-R. Chang, *et al.*, “Observation of the nonlinear Hall effect under time-reversal-symmetric conditions”, *Nature* **565**, 337 (2019).

[4] Z. Z. Du, C. M. Wang, H.-Z. Lu, and X. C. Xie, “Band signatures for strong nonlinear Hall effect in bilayer WTe₂”, *Phys. Rev. Lett.* **121**, 266601 (2018).

[5] K. Kang, T. Li, E. Sohn, J. Shan, and K. F. Mak, “Observation of the nonlinear anomalous Hall effect in few-layer WTe₂”, *Nat. Mater.* **18**, 324 (2019).

[6] Z. Z. Du, C. M. Wang, S. Li, H.-Z. Lu, and X. C. Xie, “Disorder-induced nonlinear Hall effect with time-reversal symmetry”, *Nat. Commun.* **10**, 3047 (2019).

[7] S. Nandy and I. Sodemann, “Symmetry and quantum kinetics of the nonlinear Hall effect”, *Phys. Rev. B* **100**, 195117 (2019).

[8] C. Xiao, Z. Z. Du, and Q. Niu, “Theory of nonlinear Hall effects: Modified semiclassics from quantum kinetics”, *Phys. Rev. B* **100**, 165422 (2019).

[9] H. Isobe, S.-Y. Xu, and L. Fu, “High-frequency rectification via chiral Bloch electrons”, *Sci. Adv.* **6**, eaay2497 (2020).

[10] Z. Z. Du, H.-Z. Lu, and X. C. Xie, “Nonlinear Hall effects”, *Nat. Rev. Phys.* **3**, 744 (2021).

[11] Z. Z. Du, C. M. Wang, H.-P. Sun, H.-Z. Lu, and X. C. Xie, “Quantum theory of the nonlinear Hall effect”, *Nat. Commun.* **12**, 5038 (2021).

[12] D. Kumar, C.-H. Hsu, R. Sharma, T.-R. Chang, P. Yu, J. Wang, G. Eda, G. Liang, and H. Yang, “Room-temperature nonlinear Hall effect and wireless radiofrequency rectification in Weyl semimetal TaIrTe₄”, *Nat. Nanotechnol.* **16**, 421 (2021).

[13] S.-C. Ho, C.-H. Chang, Y.-C. Hsieh, S.-T. Lo, B. Huang, T.-H.-Y. Vu, C. Ortix, and T.-M. Chen, “Hall effects in artificially corrugated bilayer graphene without breaking time-reversal symmetry”, *Nat. Electron.* **4**, 116 (2021).

[14] P. He, H. Isobe, D. Zhu, C.-H. Hsu, L. Fu, and H. Yang, “Quantum frequency doubling in the topological insulator Bi₂Se₃”, *Nat. Commun.* **12**, 1 (2021).

[15] H. Watanabe and Y. Yanase, “Nonlinear electric trans-

port in odd-parity magnetic multipole systems: Application to Mn-based compounds”, *Phys. Rev. Res.* **2**, 043081 (2020).

[16] A. Tiwari, F. Chen, S. Zhong, E. Druke, J. Koo, A. Kaczmarek, *et al.*, “Giant c-axis nonlinear anomalous Hall effect in T_d-MoTe₂ and WTe₂”, *Nat. Commun.* **12**, 2049 (2021).

[17] E. J. König and A. Levchenko, “Quantum kinetics of anomalous and nonlinear Hall effects in topological semimetals”, *Ann. Phys.* **435**, 168492 (2021).

[18] J. Duan, Y. Jian, Y. Gao, H. Peng, J. Zhong, Q. Feng, J. Mao, and Y. Yao, “Giant second-order nonlinear Hall effect in twisted bilayer graphene”, *Phys. Rev. Lett.* **129**, 186801 (2022).

[19] P. He, G. K. W. Koon, H. Isobe, J. Y. Tan, J. Hu, A. H. C. Neto, L. Fu, and H. Yang, “Graphene moiré superlattices with giant quantum nonlinearity of chiral Bloch electrons”, *Nat. Nanotechnol.* **17**, 378 (2022).

[20] M. Huang, Z. Wu, J. Hu, X. Cai, E. Li, L. An, *et al.*, “Giant nonlinear Hall effect in twisted bilayer WSe₂”, *Natl. Sci. Rev.* **10**, nwac232 (2022).

[21] D. Kaplan, T. Holder, and B. Yan, “General nonlinear Hall current in magnetic insulators beyond the quantum anomalous Hall effect”, *Nat. Commun.* **14**, 3053 (2023).

[22] L. Min, H. Tan, Z. Xie, L. Miao, R. Zhang, S. H. Lee, *et al.*, “Strong room-temperature bulk nonlinear Hall effect in a spin-valley locked Dirac material”, *Nat. Commun.* **14**, 364 (2023).

[23] D. Kaplan, T. Holder, and B. Yan, “Unification of nonlinear anomalous Hall effect and nonreciprocal magnetoresistance in metals by the quantum geometry”, *Phys. Rev. Lett.* **132**, 026301 (2024).

[24] R. Chen, Z. Z. Du, H.-P. Sun, H.-Z. Lu, and X. C. Xie, “Nonlinear Hall effect on a disordered lattice”, *Phys. Rev. B* **110**, L081301 (2024).

[25] Y. D. Wang, Z. F. Zhang, Z.-G. Zhu, and G. Su, “Intrinsic nonlinear Ohmic current”, *Phys. Rev. B* **109**, 085419 (2024).

[26] L. Xiang and J. Wang, “Intrinsic in-plane magnetononlinear Hall effect in tilted Weyl semimetals”, *Phys. Rev. B* **109**, 075419 (2024).

[27] C. Chen, D. Zhai, C. Xiao, and W. Yao, “Crossed nonlinear dynamical Hall effect in twisted bilayers”, *Phys. Rev. Res.* **6**, L012059 (2024).

[28] J. Yao, Y. Liu, and W. Duan, “Geometrical nonlinear Hall effect induced by Lorentz force”, *Phys. Rev. B* **110**, 115123 (2024).

[29] P. He, H. Isobe, G. K. W. Koon, J. Y. Tan, J. Hu, J. Li, N. Nagaosa, and J. Shen, “Third-order nonlinear Hall effect in a quantum Hall system”, *Nat. Nanotechnol.* (2024), 10.1038/s41565-024-01730-1.

[30] Y. Gao, S. A. Yang, and Q. Niu, “Field induced positional shift of Bloch electrons and its dynamical implications”, *Phys. Rev. Lett.* **112**, 166601 (2014).

[31] C. Wang, Y. Gao, and D. Xiao, “Intrinsic nonlinear Hall effect in antiferromagnetic tetragonal CuMnAs”, *Phys. Rev. Lett.* **127**, 277201 (2021).

[32] H. Liu, J. Zhao, Y.-X. Huang, W. Wu, X.-L. Sheng, C. Xiao, and S. A. Yang, “Intrinsic second-order anomalous Hall effect and its application in compensated antiferromagnets”, *Phys. Rev. Lett.* **127**, 277202 (2021).

[33] A. Gao, Y.-F. Liu, J.-X. Qiu, B. Ghosh, T. V. Trevisan, Y. Onishi, *et al.*, “Quantum metric nonlinear Hall effect in a topological antiferromagnetic heterostructure”, *Sci-*

ence **381**, 181 (2023).

[34] N. Wang, D. Kaplan, Z. Zhang, T. Holder, N. Cao, A. Wang, *et al.*, “Quantum-metric-induced nonlinear transport in a topological antiferromagnet”, *Nature* **621**, 487 (2023).

[35] Y. Fang, J. Cano, and S. A. A. Ghorashi, “Quantum geometry induced nonlinear transport in altermagnets”, *Phys. Rev. Lett.* **133**, 106701 (2024).

[36] J. Provost and G. Vallee, “Riemannian structure on manifolds of quantum states”, *Commun. Math. Phys.* **76**, 289 (1980).

[37] R. Resta, “The insulating state of matter: a geometrical theory”, *Eur. Phys. J. B* **79**, 121 (2011).

[38] P. Törmä, S. Peotta, and B. A. Bernevig, “Superconductivity, superfluidity and quantum geometry in twisted multilayer systems”, *Nat. Rev. Phys.* **4**, 528 (2022).

[39] P. Törmä, “Essay: Where can quantum geometry lead us?”, *Phys. Rev. Lett.* **131**, 240001 (2023).

[40] A. Bouhon, A. Timmel, and R.-J. Slager, “Quantum geometry beyond projective single bands”, [arXiv:2303.02180](https://arxiv.org/abs/2303.02180) (2023).

[41] T. Liu, X.-B. Qiang, H.-Z. Lu, and X. C. Xie, “Quantum geometry in condensed matter”, *Natl. Sci. Rev.* , nwae334 (2024).

[42] N. Nagaosa, J. Sinova, S. Onoda, A. H. MacDonald, and N. P. Ong, “Anomalous Hall effect”, *Rev. Mod. Phys.* **82**, 1539 (2010).

[43] D. Ma, A. Arora, G. Vignale, and J. C. W. Song, “Anomalous skew-scattering nonlinear Hall effect and chiral photocurrents in \mathcal{PT} -symmetric antiferromagnets”, *Phys. Rev. Lett.* **131**, 076601 (2023).

[44] R. B. Atencia, D. Xiao, and D. Culcer, “Disorder in the nonlinear anomalous Hall effect of \mathcal{PT} -symmetric Dirac fermions”, *Phys. Rev. B* **108**, L201115 (2023).

[45] D. Xiao, M. C. Chang, and Q. Niu, “Berry phase effects on electronic properties”, *Rev. Mod. Phys.* **82**, 1959 (2010).

[46] See Supplemental Materials for the detailed calculations.

[47] N. A. Siniatsyn, “Semiclassical theories of the anomalous Hall effect”, *J. Phys. Condens. Matter* **20**, 023201 (2008).

[48] G. D. Mahan, *Many-Particle Physics* (Plenum Press, 1990).

[49] R. B. Atencia, Q. Niu, and D. Culcer, “Semiclassical response of disordered conductors: Extrinsic carrier velocity and spin and field-corrected collision integral”, *Phys. Rev. Res.* **4**, 013001 (2022).

[50] H. Liu, J. H. Cullen, and D. Culcer, “Topological nature of the proper spin current and the spin-Hall torque”, *Phys. Rev. B* **108**, 195434 (2023).

[51] M. Mehraeen, “Quantum kinetic theory of quadratic responses”, [arXiv:2409.14539](https://arxiv.org/abs/2409.14539) (2024).

[52] Z.-F. Zhang, Z.-G. Zhu, and G. Su, “Symmetry dictionary on charge and spin nonlinear responses for all magnetic point groups with nontrivial topological nature”, *Natl. Sci. Rev.* **10**, nwad104 (2023).

[53] G.-B. Liu, Z. Zhang, Z.-M. Yu, and Y. Yao, “Msgcorep: A package for corepresentations of magnetic space groups”, *Comput. Phys. Commun.* **288**, 108722 (2023).

[54] H.-P. Sun, C. M. Wang, S.-B. Zhang, R. Chen, Y. Zhao, C. Liu, Q. Liu, C. Chen, H.-Z. Lu, and X. C. Xie, “Analytical solution for the surface states of the antiferromagnetic topological insulator MnBi_2Te_4 ”, *Phys. Rev. B* **102**, 241406 (2020).

[55] Y. Tian, L. Ye, and X. Jin, “Proper scaling of the anomalous Hall effect”, *Phys. Rev. Lett.* **103**, 087206 (2009).

[56] D. Hou, G. Su, Y. Tian, X. Jin, S. A. Yang, and Q. Niu, “Multivariable scaling for the anomalous Hall effect”, *Phys. Rev. Lett.* **114**, 217203 (2015).

[57] Y.-X. Huang, C. Xiao, S. A. Yang, and X. Li, “Scaling law for time-reversal-odd nonlinear transport”, [arXiv:2311.01219](https://arxiv.org/abs/2311.01219) (2023).